CHALMERS

UNIVERSITY OF TECHNOLOGY

Interplay of NH4+ and BH4- reorientational dynamics in NH4BH4

(article starts on next page)

Interplay of NH_4^+ and BH_4^- reorientational dynamics in NH_4BH_4

Mikael S. Andersson,[1,2,*] Jakob B. Grinderslev,[3] Torben R. Jensen,[3] Victoria García Sakai ●,[4] Ulrich Häussermann,[5] Terrence J. Udovic ●,[2,6] and Maths Karlsson ●[1]

[1]*Department of Chemistry and Chemical Engineering, Chalmers University of Technology, Göteborg SE-412 96, Sweden*
[2]*NIST Center for Neutron Research, National Institute of Standards and Technology, Gaithersburg, Maryland 20899-6102, USA*
[3]*Interdisciplinary Nanoscience Center (iNANO) and Department of Chemistry,*
Aarhus University, DK-8000 Aarhus, Denmark
[4]*ISIS Neutron and Muon Source, STFC Rutherford Appleton Laboratory, Oxfordshire OX11 0QX, United Kingdom*
[5]*Department of Materials and Environmental Chemistry, Stockholm University, SE-10691 Stockholm, Sweden*
[6]*Department of Materials Science and Engineering, University of Maryland, College Park, Maryland 20742-2115, USA*

The reorientational dynamics of ammonium borohydride (NH_4BH_4) was studied using quasielastic neutron scattering in the temperature interval from 10 to 240 K, which covers both the dynamically ordered and disordered polymorphs of NH_4BH_4. In the low-temperature (< 50 K) ordered polymorph of NH_4BH_4, analysis of the quasielastic neutron scattering data reveals that no reorientational dynamics is present within the probed timescale region of 0.1 to 100 ps. In the high-temperature (> 50 K) disordered polymorph, the analysis establishes the onset of NH_4^+ and BH_4^- dynamics at around 50 and 125 K, respectively. The relaxation time at 150 K for NH_4^+ is approximately 1 ps, while around 100 ps for BH_4^-. The NH_4^+ dynamics at temperatures below 125 K is associated with preferential tetrahedral tumbling motions, where each of the hydrogen atoms in the NH_4^+ tetrahedron can visit any of the four hydrogen sites, however, reorientations around a specific axis are more frequently occurring (C_2 or C_3). At higher temperatures, the analysis does not exclude a possible evolution of the NH_4^+ dynamics from tetrahedral tumbling to either cubic tumbling, where the hydrogen atoms can visit any of the eight positions corresponding to the corners of a cube, or isotropic rotational diffusion, where the hydrogen atoms can visit any location on the surface of a sphere. The BH_4^- dynamics can be described as cubic tumbling. The difference in reorientational dynamics between the two ions is related to the difference of the local environment where the dynamically much slower BH_4^- anion imposes a noncubic environment on the NH_4^+ cation.

I. INTRODUCTION

Ammonium borohydride, NH_4BH_4, was first synthesized in the late 1950s [1], but it is once again receiving attention due to its high gravimetric (24.5 wt.%) and volumetric (157 g H_2/L) hydrogen densities and concomitant relevance as a hydrogen storage material [2–4]. A critical parameter toward practical applications of these types of materials is the binding energy (or thermal stability) for hydrogen, which should allow its absorption and desorption near room temperature at atmospheric pressure. NH_4BH_4 is, impractically, thermally stable only below 230 K. An increase of the temperature range of thermal stability for NH_4BH_4 through modification depends on a thorough understanding of the structure and

dynamics underpinning the hydrogen sorption process in this material, but such an understanding is at present lacking.

Powder x-ray diffraction measurements at 100 K indicated that NH_4BH_4 exhibits a cubic crystal structure (space group Fm-$3m$) with the two tetrahedral complex ions, ammonium (NH_4^+) and borohydride (BH_4^-), which may be described as cubes with half occupancies of hydrogen due to disorder (see Supplemental Material (SM), Fig. S1 [5])[3,6]. Variable-temperature neutron powder diffraction measurements on the deuterated equivalent ND_4BD_4 showed that, at 5 K, ND_4BD_4 exhibits a dynamically ordered trigonal polymorph (P-3), which transforms to a rhombohedral polymorph (R-$3m$) at 45 K, which in turn transforms to the cubic high-temperature polymorph (Fm-$3m$) at 60 K [7]. Furthermore, the neutron diffraction data provided insight into the H(D) positions in the structure. In particular, while the neutron data confirmed the hydrogen positions for BH_4^- as determined from x-ray diffraction analysis, it suggests a multitude of different orientations for the NH_4^+ cations in the cubic polymorph [see Fig. 1(a)] [7,8]. However, it is not clear whether the apparent cation and anion disorder are purely static or dynamic in nature.

A powerful method to study the nature of dynamical disorder in these polymorphs is quasielastic neutron scattering

*anmikael@chalmers.se

(a)

(b)   (c)   (d)

Cubic
Tumbling

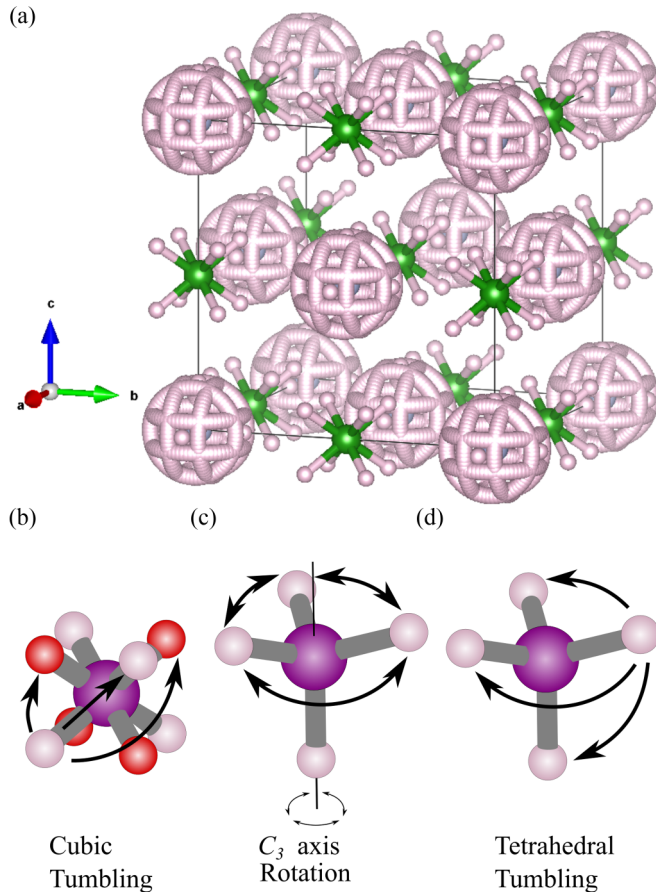C_3 axis
Rotation

Tetrahedral
Tumbling

FIG. 1. (a) Crystal structure of the cubic polymorph of NH_4BH_4 (Fm-$3m$), showing the cubic distribution of H positions for BH_4^- and a multitude of H positions for NH_4^+. The structure has been plotted based on the atomic positions given in Ref. [7]. (b)–(d) Show schematic representations of different reorientational motions of the NH_4^+ and BH_4^- tetrahedral ions. (b) Cubic tumbling: each of the hydrogen atoms can visit any of the eight positions corresponding to the corners of a cube. This corresponds to two orientations of the tetrahedron with a relative rotation of 90° around a C_2 axis. The hydrogen corresponding to the two tetrahedra have been color coded differently (pink/red) for emphasis. (c) C_3 axis rotation: three of the hydrogen atoms perform 120° jumps around a ring, while the fourth hydrogen atom remains in the same position. (d) Tetrahedral tumbling: each of the hydrogen atoms can visit any of the four positions in the tetrahedron. Color scheme: green (boron), pink/red (hydrogen), purple (boron or nitrogen).

(QENS). Since QENS is sensitive to incoherent scattering and because hydrogen has a very large incoherent scattering cross section, the QENS signal is generally dominated by hydrogen scattering for hydrogen containing compounds such as borohydrides. Previous QENS studies on borohydrides have mainly focused on materials with only one active species (NH_4^+ or BH_4^-), such as in the compounds $LiBH_4$, $NaBH_4$, KBH_4, and $(NH_4)_2B_{12}H_{12}$. For the two cubic compounds (Fm-$3m$) $NaBH_4$ and KBH_4 (isostructural to NH_4BH_4), it was shown that the tetrahedral BH_4^- anion can reorient so that each hydrogen can visit any of the eight positions on the corners of a cube (cubic tumbling) [see Fig. 1(b)] [9]. For the orthorhombic polymorph of $LiBH_4$ ($Pnma$), it was shown that the BH_4^-

anion makes threefold (C_3) rotations around a single B-H axis, so that one H atom remains static, while the remaining three H atoms make a threefold rotation on a circle perpendicular to the B-H axis [see Fig. 1(c)] [10]. A related study on NH_4^+ dynamics in the cubic polymorph of $(NH_4)_2B_{12}H_{12}$, where the NH_4^+ ions have a tetrahedral local environment, showed that the NH_4^+ tetrahedron assumes one orientation only, however, with the possibility of each hydrogen atom visiting any of the four positions in the tetrahedron (tetrahedral tumbling) [see Fig. 1(d)] [11]. In the above-mentioned compounds, the nature of the dynamics is strongly correlated to the local environment of the respective compound.

For NH_4BH_4, it is expected that both ions (NH_4^+ and BH_4^-) are dynamically active and that possibly their dynamics are dependent on each other. Furthermore, NH_4BH_4 exhibits different polymorphs (P-3, R-3m, Fm-3m) depending on the temperature, which could mean significant differences in the dynamics as a result of the structural differences. A combined *ab initio* molecular dynamics (MD) simulation and solid-state nuclear magnetic resonance (ssNMR) study of NH_4BH_4 at room temperature indicated that both the cations and the anions undergo rapid reorientations, with the BH_4^- anion being slightly more hindered than the NH_4^+ cation. The spatial geometry of the observed dynamics was, however, found to be inconclusive as it could be interpreted as either cubic tumbling, rotational diffusion on a sphere, or reorientation between tetrahedral sites (tetrahedral tumbling) [6]. Subsequent results from QENS experiments on the cubic high-temperature polymorph of ND_4BH_4, NH_4BD_4, and NH_4BH_4 indicated that both NH_4^+ and BH_4^- reorient around either its C_2 or C_3 axis [8]. However, because of a limitation of the probed range of momentum transfers (Q), it was not possible to differentiate between some of the proposed reorientational mechanisms and, furthermore, two timescales were detected for the NH_4^+ cation reorientation, which is inconsistent with C_2 or C_3 reorientations [12]. Thus, it is of importance to obtain more information on this topic. Toward this aim, we present a systematic QENS study of the dynamical behavior of NH_4^+ and BH_4^- in NH_4BH_4 over an extended Q range, as well as over a large temperature interval ranging from 10 to 240 K. Analysis of the QENS data establishes the onset of NH_4^+ reorientational dynamics undergoing preferential tetrahedral tumbling motions above 50 K while not excluding a possible evolution to either cubic tumbling or isotropic rotational diffusion motions above 125 K. The analysis also suggests that the BH_4^- anions undergo a cubic tumbling motion above 125 K. Thus, it can be established that the diffraction-observed disorder is of a dynamical nature.

II. EXPERIMENTS

A. Materials synthesis

A ^{11}B-enriched sample of NH_4BH_4 was prepared following previously published procedures [3,13]. Initially, $Na^{11}BH_4$ was synthesized from NaH (Dry, 95%, Sigma Aldrich) [14] and $S(CH_3)_2$ $^{11}BH_3$ (10 M, Katchem). First, NaH was mechanochemically activated by ball milling using a Fritsch Pulverisette 6 planetary ball mill. The powdered NaH was loaded into a 80-mL tungsten carbide vial with tungsten

carbide balls (5.5 g each) with a ball-to-powder weight ratio of 30:1, and sealed in an argon-filled glovebox. The powder was milled at 350 rpm and a milling time of 10×10 min interrupted by 2-min breaks, resulting in a total milling time of 100 min. The activated NaH was mixed with S(CH$_3$)$_2$ ^{11}BH$_3$ (50% molar excess) and diluted to 5 mol/L using toluene (anhydrous, Sigma Aldrich). After 7 d of stirring at 333 K, Na^{11}BH$_4$ was synthesized. NH$_4^{11}$BH$_4$ was synthesized from NH$_4$F ($\geqslant$99.99%, Sigma Aldrich) and Na^{11}BH$_4$. NH$_4$F (10% molar excess) and Na^{11}BH$_4$ were reacted in liquid NH$_3$ while stirring at 195 K (dry ice/ethanol). NH$_4^{11}$BH$_4$ is formed after 4 h. The by-products, NaF and unreacted NH$_4$F, were removed by filtration. Excess NH$_3$ was removed under dynamic vacuum at 233 K to recover NH$_4^{11}$BH$_4$ as a white polycrystalline powder.

B. X-ray powder diffraction

The powder sample was investigated by synchrotron x-ray powder diffraction (XRPD) at room temperature using the MS-powder beamline at the Swiss Light Source (SLS), PSI, Switzerland, using $\lambda = 0.710\,162$ Å and employing a MYTHEN detector [15]. Rietveld refinement of the XRPD data showed that NH$_4$BH$_4$ crystallizes in the NaCl-type structure with space-group symmetry Fm-3m and thus replicating the results in Ref. [6] (see SM, Fig. S1 [5]). Further details about the XRPD analysis are given in Ref. [16].

C. Quasielastic neutron scattering

The QENS measurements were performed on OSIRIS [17] at the ISIS Neutron and Muon Source in the U.K. Two different analyzers (PG 002 and PG 004, respectively) were used for the measurements. PG 002 has a full width at half-maximum (FWHM) of 25 μeV and a maximum energy window of ± 0.4 meV, while PG 004 has a FWHM of 100 μeV and a maximum energy window of -3 meV to $+4$ meV. Using a combination of these two analyzers allowed studies of dynamic processes with relaxation times in the picosecond regime.

The powder sample was evenly distributed in an aluminum foil pouch, which was wrapped in an annular shape and placed into a double-walled, annular aluminum can sealed using an indium O-ring. During the entire sample preparation, the sample was kept cold (using either dry ice or liquid nitrogen) and in an inert Ar atmosphere to avoid decomposition of the sample. The sample can was inserted into the OSIRIS cryostat at a temperature of 200 K. The measurements were then performed at temperatures from 10 to 240 K, with the heating and cooling rates kept low (1–2 K/min), to avoid freezing in any metastable polymorphs [7,8]. Specifically, spectra were measured at 10, 20, 30, 40, 45, 50, 55, 60, 65, 70, 75, 80, 90, 100, 110, 125, 140, 150, 160, 175, 190, 200, 210, 220, 230, and 240 K, using the PG 002 analyzer, and at 10, 60, 80, 100, 125, 150, 175, and 200 K, using the PG 004 analyzer.

The obtained quantity from the QENS measurements is the scattering function

$$S(Q, \omega) = R(Q, \omega) \otimes \left[\delta(\omega)A_{\mathrm{E}}(Q) + \sum_i L_i(\omega)A_{\mathrm{QE},i}(Q) \right],$$

(1)

where $E = \hbar\omega$ is the neutron energy transfer, $\hbar$ is the Planck constant$/(2\pi)$, ω is the angular frequency, δ is a delta function, L_i's are Lorentzian functions used to describe the quasielastic scattering, and A_{E} and $A_{\mathrm{QE},i}$ are the areas corresponding to the respective delta and Lorentzian functions. The delta and Lorentzian functions are convoluted with the instrument resolution function $R(Q, \omega)$. Using the scattering function presented above, the data were fitted using a delta function to describe the elastic scattering, and one or more Lorentzians to describe the quasielastic scattering. Furthermore, a linear function was used for the background. The data were reduced using MANTID [18] and analyzed using PAN which is included in the DAVE distribution [19].

III. RESULTS AND DISCUSSION

A. Elastic and inelastic fixed window scans

Elastic fixed window scans (EFWS) and inelastic fixed window scans (IFWS) were simultaneously collected during heating. In an EFWS experiment, the intensity of a narrow energy slice centered at the elastic peak position is integrated for each individual temperature. As the dynamics develop on the instrumental timescale, the integrated intensity will decrease since the quasielastic component becomes broader than, and collapses under, the elastic peak (± 25 μeV) and the total scattering intensity (sum of elastic and quasielastic) is constant. For the IFWS, an energy slice is chosen away from the elastic peak (50 to 100 μeV). The dynamics come into the energy slice window as the quasielastic component broadens. Thus, the integrated FWS intensity will initially increase. Yet, as the dynamics develops further, the quasielastic component will become even broader and the intensity will start to decrease since the quasielastic intensity will be distributed over a larger energy region, outside of the chosen energy window.

Figure 2 shows the EFWS and IFWS in the temperature range from 10 to 240 K. For temperatures up to 50 K, we observe no significant change in the intensity for either the EFWS or the IFWS, indicating that the dynamics is "frozen" within the probed range of timescales. While no significant change in the intensity occurs in this temperature region, a minor change due to the Debye-Waller factor is observed. Upon further heating, the EFWS starts to rapidly decrease until it reaches a plateau at around 125 K [Fig. 2(a)], which is observed as a peak and a valley in the IFWS [Fig. 2(b)]. The observation of a decreasing EFWS and increasing IFWS is in accordance with the onset of one or several dynamical processes. Notably, we observe that the onset of dynamics occurs at the first-order polymorphic transition of NH$_4$BH$_4$ [7,8], which is associated with the transformation of the tetrahedral NH$_4^+$ cation from a reorientationally ordered state at low temperature to a disordered state upon heating. This suggests that the dynamics in the 50 to 125 K regime primarily reflects reorientational dynamics of NH$_4^+$ [7,8,16]. At temperatures higher than 125 K, the EFWS starts to once again decrease, while a second peak is observed in the IFWS at around 200 K. This behavior corresponds to the onset of a second dynamical process, in addition to the NH$_4^+$ reorientational dynamics, which we attribute to BH$_4^-$ reorientational motions. This is consistent with the similar onset
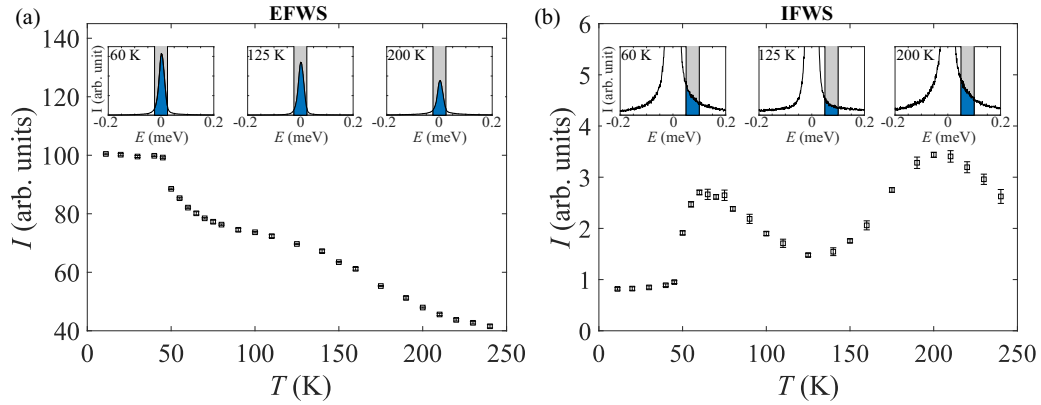
FIG. 2. (a) EFWS and (b) IFWS of NH_4BH_4, with the integrated areas for a selection of temperatures indicated in the insets. The bounds for integration are ± 25 μeV in (a) and 50-100 μeV in (b). Error bars are one standard deviation.

temperature for BH_4^- reorientational dynamics in isostructural KBH_4 and $RbBH_4$ [20].

B. Quasielastic neutron scattering spectra

Figure 3 shows several high-resolution QENS measurements (PG 002) made between 10 and 80 K, whereas the spectra at higher temperatures (100–200 K) are shown in the SM, Fig. S2 [5]. No significant change was observed upon heating from 10 to 45 K, while a noticeable change occurred between 45 and 50 K. Only minor changes were observed upon further heating. From this we can infer that NH_4^+ dynamics is frozen out below 50 K and that there is a drastic change in the relaxation time between 45 and 50 K, leading to the sharp onset of the observed dynamics as also shown by the EFWS and IFWS data presented in Fig. 2. The change in relaxation time is estimated to be a factor of 50 or more since no broadening could be detected at 45 K (smallest detectable width using the PG002 analyzer is ≈ 0.01 meV), while a width of 0.5 meV was determined for 50 K. One

FIG. 3. QENS spectra of NH_4BH_4 obtained at different temperatures. The spectra have been integrated over the Q range of 0.18–1.81 Å^{-1}.

should note that while previous neutron diffraction studies indicated the transformation from a rhombohedral polymorph at 45–60 K to a cubic polymorph at 60 K [7,8], no particular features are observed here and were also not detected in our recent vibrational spectroscopy study [16]. Nevertheless, in order to avoid complications related to a possible polymorphic transition, we focus our study of the QENS spectra higher than 60 K.

In our more detailed analysis, we find that the 60–100 K spectra can be well approximated according to Eq. (1) using two Lorentzian components; Fig. 4(a) shows the fit to the QENS spectrum at 100 K and $Q = 3.46$ Å^{-1}. The need for two Lorentzian functions to describe the spectra suggests that there are two relaxation processes present in the system. Based on the FWSs (Fig. 2), it is expected that the BH_4^- reorientations will be frozen below 125 K. Hence, these relaxation processes relate to NH_4^+ dynamics only. At higher temperatures (>125 K), the fit to the QENS spectra requires three Lorentzians [Fig. 4(b)]. This is in full accordance with the onset of considerable BH_4^- reorientational dynamics at around 125 K, thus meaning that the NH_4^+ and BH_4^- dynamics occur simultaneously on the probed timescales. To determine the spatial geometry of the observed dynamics, we analyze the elastic incoherent structure factor (EISF).

C. Elastic incoherent structure factors

The EISF has been determined experimentally by taking the ratio of the elastic (incoherent) scattering intensity to the total (incoherent) scattering intensity, for the different Q values, where the total incoherent scattering intensity is the sum of the intensities of the elastic and quasielastic scattering. Thus, the ESIF can be expressed as

$$\text{EISF} = \frac{A_E(Q)}{A_E(Q) + A_{QE}(Q)}, \quad (2)$$

where $A_E(Q)$ and $A_{QE}(Q)$ are the total elastic and quasielastic integrated scattering intensities for a specific value of Q. The minimum of the EISF is dependent on the ratio of atoms undergoing reorientation. Furthermore, the position of this minimum in Q is dependent on the reorientational jump distance [see SM for further information [5]].
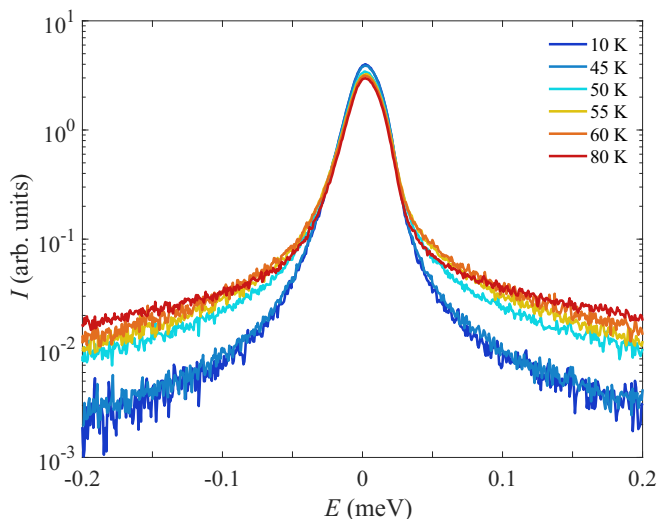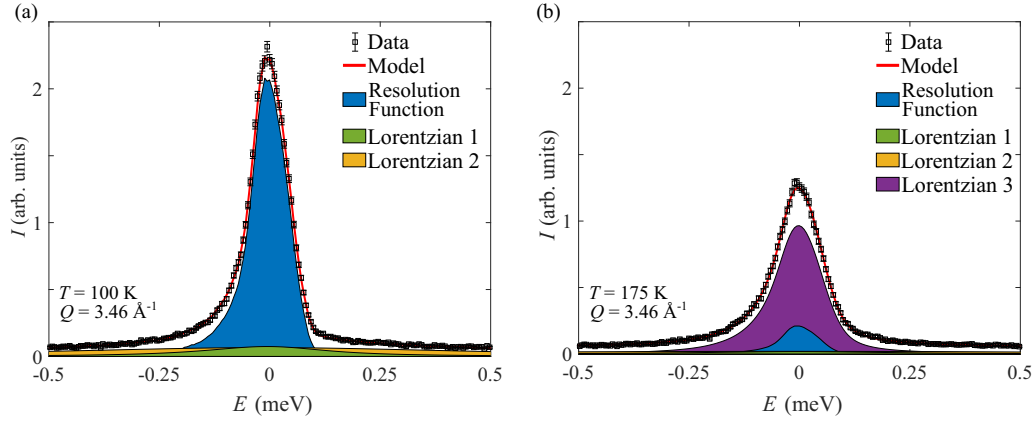
FIG. 4. QENS spectra and corresponding fits of $S(Q,\omega)$ for NH$_4$BH$_4$ at $Q = 3.46$ Å^{-1} and at $T = 100$ and 175 K. Error bars are one standard deviation.

D. NH$_4^+$ reorientational dynamics

Figure 5(a) presents the experimentally determined EISF at 100 K and based on the position of the minimum and the magnitude of this EISF it can be concluded that only NH$_4^+$ reorientational dynamics occurs at this temperature. The experimentally determined EISF is compared with calculated EISF models associated with possible reorientational mechanisms, namely, C_2 or C_3 reorientation [21], tetrahedral tumbling [22], cubic tumbling [23], and isotropic rotational diffusion on a sphere. The five EISF functions were chosen based on the tetrahedral geometry of the NH$_4^+$ and BH$_4^-$ ions and of the cubic geometry of the crystal structure. Mathematical expressions for the different EISF models are given in the SM [5]. The EISF models were adjusted to include the four static hydrogen atoms of BH$_4^-$, resulting in the following expression:

$$\text{EISF}_{\text{total}} = \tfrac{4}{8} + \tfrac{4}{8}\text{EISF}_{\text{NH}_4^+}. \tag{3}$$

Although diffraction results have indicated the possibility that NH$_4^+$ ions are fully orientationally disordered and undergo isotropic rotational diffusion [7,8], the best agreement between data and model was found for the reorientational jump mechanism corresponding to NH$_4^+$ tetrahedral tumbling. Tetrahedral tumbling normally exhibits only one relaxation time (or jump frequency), however, the two Lorentzians required to fit the spectra suggest that two different jump frequencies are involved in the observed tumbling motion. To examine this, the EISF resulting from only the higher-frequency motion (i.e., the broader Lorentzian component), can be defined as

$$\text{EISF} = \frac{A_\text{E}(Q) + A_{\text{QE, slow}}(Q)}{A_\text{E}(Q) + A_{\text{QE, slow}}(Q) + A_{\text{QE, fast}}(Q)}. \tag{4}$$

This would correspond to an experiment made using a lower-energy resolution, where the slower component would be buried in the elastic peak, leaving only the broader quasielastic Lorentzian component. A good agreement is found between
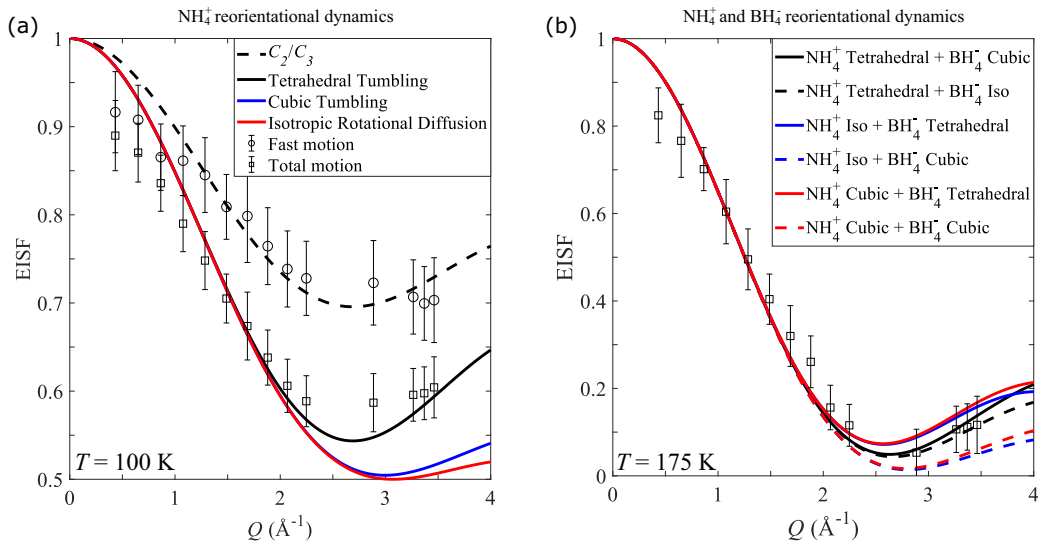

FIG. 5. (a) EISF at 100 K corresponding to the faster (C_2 or C_3 uniaxial reorientation) and the total motion (tetrahedral tumbling) = fast + slow motion of the NH$_4^+$ cations. (b) EISF corresponding to the concurrent motions of NH$_4^+$ and BH$_4^-$ at 175 K. The error bars are two standard deviations. Data in the Q regions of 2.4–2.85 Å^{-1} and 3–3.25 Å^{-1} have been removed because of the contamination from Bragg peaks.

the derived EISF and a reorientational mechanism involving uniaxial rotations around either a twofold (C_2) or threefold symmetry axis (C_3), in agreement with previous investigations [see Fig. 5(a)] [8]. The EISFs for the C_2 and C_3 reorientations are identical for a tetrahedral ion, which means it is not possible to differentiate between the two mechanisms. Although it is clear from this finding that each of the hydrogen atoms of any particular NH_4^+ cation can visit all of the four hydrogen positions of the tetrahedron, it is also clear that the hydrogen will more frequently undergo a uniaxial motion corresponding to a C_2 or C_3 rotation. It follows that there is a preferential axis of rotation for NH_4^+.

In order to confirm the effect on the EISF corresponding to tetrahedral tumbling when introducing a preferential axis rotation, we have derived the scattering function $S(Q, \omega)$ for tetrahedral tumbling with one preferred faster C_3 axis of rotation. This corresponds to the case where jumps around this preferred C_3 axis ring [Fig. 1(c)] are relatively fast while jumps to and from the ring involving reorientations around the other three C_3 symmetry axes are relatively slow; see SM for details [5]. Since all four hydrogen sites have full occupancy, jumps to and from the ring have the same (slow) relaxation time, while jumps around the ring have the same (fast) relaxation time and $S(Q, \omega)$ therefore takes the form

$$S(Q, \omega) = \frac{1 + 3 j_0(Qd)}{4\pi}\delta + \frac{1 - j_0(Qd)}{4\pi}$$
$$\times \left(\frac{4/\alpha\tau}{[4/\alpha\tau]^2 + \omega^2} + 2\frac{(1+3\alpha)/\alpha\tau}{[(1+3\alpha)/\alpha\tau]^2 + \omega^2} \right),$$
(5)

where j_0 is the zeroth-order spherical Bessel function, d the jump distance, and the relaxation times of the fast (τ_{fast}) and slow (τ_{slow}) motions are connected as $\alpha\tau_{\text{fast}} = \tau_{\text{slow}}$ with $\infty > \alpha \geqslant 1$. In the case of $\alpha \to \infty$, which corresponds to a jump rate ($1/\tau$) slower than the instrumental resolution, $S(Q, \omega)$ can be expressed as

$$S(Q, \omega) = \frac{2 + 2 j_0(Qd)}{4\pi}\delta + \frac{2(1 - j_0(Qd))}{4\pi}\frac{3/\tau}{(3/\tau)^2 + \omega^2},$$
(6)

which is exactly the expected $S(Q, \omega)$ for uniaxial C_3 axis reorientation of a tetrahedral ion. In the case of $\infty > \alpha \geqslant 1$, the EISF is unaffected by α, which means that no matter how different the relaxation times are for visiting all of the sites in the tetrahedron, the EISF is relaxation-time independent as long as all of the quasielastic components (timescales) can be resolved. This justifies the use of a tetrahedral tumbling model, even though two relaxation times were needed to accurately describe the data.

As mentioned earlier, from the diffraction-derived disordered cubic structure in Refs. [7,8], a high degree of orientational disorder is implied for the NH_4^+ cations, while only eight hydrogen positions are implied for the BH_4^- anions [see Fig. 1(a)]. Since the apparent high degree of NH_4^+ disorder does not portend the observed tetrahedral tumbling, this implies that the NH_4^+ cations retain a preferable tetrahedral orientation for some period of time (while undergoing many reorientational jumps) in each individual unit cell. However, these orientations can differ dramatically among the different

unit cells, leading to a diffraction-averaged spherical smearing of the H atom positions, which agrees well with the diffraction-derived disorder. These preferred NH_4^+ orientations are possible due to the distribution of different frozen orientations of the surrounding BH_4^- anions, whose eight diffraction-derived hydrogen positions per anion site indicate that two anion orientations are possible at each site.

E. Simultaneous NH_4^+ and BH_4^- dynamics

To describe the spectra at temperatures higher than 125 K, which are associated with the simultaneous NH_4^+ and BH_4^- reorientations, the EISF can be expressed as

$$\text{EISF}_{\text{total}} = \tfrac{4}{8}\text{EISF}_{NH_4^+} + \tfrac{4}{8}\text{EISF}_{BH_4^-}.$$
(7)

Figure 5(b) compares the experimental EISF with composite model curves combining the EISF for NH_4^+ tetrahedral tumbling with the EISFs corresponding to different possible BH_4^- reorientational mechanisms. From the magnitude of the experimentally determined EISF it can be concluded that both the NH_4^+ and the BH_4^- ions undergo reorientations at this temperature. As can be observed, there is a good agreement with both the cubic tumbling and the isotropic rotational diffusion mechanisms of BH_4^-. As the neutron diffraction results point toward eight distinct hydrogen locations (at the corners of a cube) for BH_4^-, the isotropic rotational diffusion mechanism can be ruled out. However, it is possible that the extra thermal energy at 175 K allows the NH_4^+ cations to undergo isotropic rotational diffusion on a sphere or cubic tumbling, instead of tetrahedral tumbling. To examine this possibility, the experimentally determined EISF was compared to composite model curves combining EISFs for the NH_4^+ cation corresponding to cubic tumbling, or isotropic rotational diffusion, respectively, with the EISFs for tetrahedral or cubic tumbling of the BH_4^- anion [see Fig. 5(b)]. While the model based on tetrahedral tumbling motion of the NH_4^+ cation and a cubic tumbling motion for the BH_4^- anion agrees best with the data, the data neither exclude the possibility that the reorientational mechanism of the NH_4^+ cations is either cubic tumbling or isotropic rotational diffusion nor that the reorientational mechanism of the BH_4^- anions is tetrahedral tumbling at this high temperature. However, all of the composite EISF models suggesting tetrahedral tumbling of the BH_4^- anions include either cubic tumbling or isotropic rotational diffusion for the NH_4^+ cations, both of which would induce a cubic local environment for the BH_4^- anions. Since the reorientational mechanism is sensitive to the local environment, it is more likely that the BH_4^- anions in a local cubic environment are undergoing cubic tumbling. However, tetrahedral tumbling cannot completely be excluded as a reorientational mechanism for the BH_4^- anions.

F. Energy barriers of the reorientational dynamics

Figure 6(a) shows the relaxation times, as extracted from the linewidths (FWHM, Γ) of each Lorentzian component ($\tau = 2\hbar/\Gamma$) as a function of temperature. Each process follows an Arrhenius behavior ($\tau = \tau_0 e^{E_b/k_B T}$), with energy barriers of $E_b = 8.6 \pm 1.2$ meV for $NH_{4,\text{fast}}^+$ dynamics, $E_b = 12.7 \pm 2.4$ meV for $NH_{4,\text{slow}}^+$ dynamics, and $E_b = 100 \pm 2$ meV for BH_4^- dynamics [see Fig. 6(a)]. Using a different
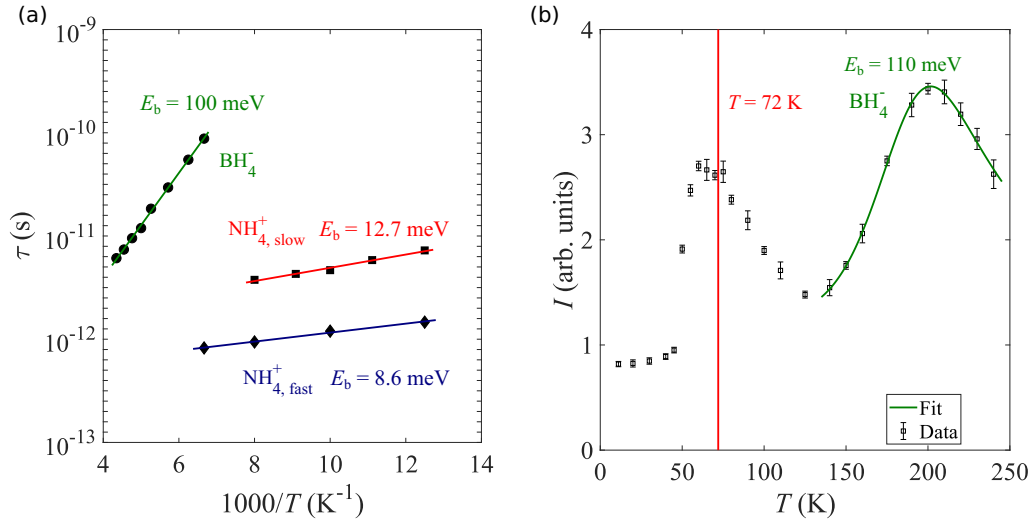
FIG. 6. (a) Arrhenius plot of the relaxation time for the $NH_{4,fast}^+$, $NH_{4,slow}^+$, and BH_4^- reorientational dynamics. (b) IFWS of NH_4BH_4 with a fit to Eq. (8) in the temperature interval 140–240 K. The red line indicates the IFWS peak position of the $NH_{4,slow}^+$ dynamics estimated using Eq. (9). Error bars are one standard deviation.

approach, we have also determined the energy barrier for BH_4^- dynamics by fitting IFWS data [Fig. 2(b)] to the following function [24]:

$$I_{\omega_{off}}^{IFWS}(T) \propto C \frac{\tau(T)}{1 + \omega_{off}^2 \tau(T)^2},$$ (8)

where C is a scaling factor, ω_{off} is the angular frequency corresponding to the chosen offset energy (75 μeV), and τ comes from the Arrhenius equation $\tau(T) = \tau_0 e^{E_b/k_B T}$. A free fit over the temperature range 140–240 K gives a very satisfactory result [see Fig. 6(b)] and yields $E_b = 110$ meV, thus in good agreement with Fig. 6(a).

Regarding a similar analysis of the energy barriers for the corresponding NH_4^+ dynamics, the fitting of the IFWS [Fig. 6(b)] proved to be difficult due to the two relaxation times involved at these temperatures and the polymorphic transition limiting the region of fitting. However, in such cases one can, instead, calculate the peak position of the IFWS intensity T_{max} from the following relationship [24]:

$$T_{max} = \frac{E_b/k_B}{\ln(\frac{1}{\omega_{off}\tau_0})}.$$ (9)

Using the extracted values for E_b (12.7 meV) and τ_0 (1.1 $\times 10^{-12}$ s), we obtain $T_{max} = 72$ K. This value is in good agreement with the observed peak position [red line in Fig. 6(b)], which shows that the values for τ_0 and E_b are robust. With regard to the literature, the energy barriers for NH_4^+ dynamics are similar to what has been observed in the related compound $(NH_4)_2B_{12}H_{12}$ (≈ 8 meV) [11], but significantly lower than found for the ammonium halides ($NH_4X; X = $ Cl, Br, or I), which have energy barriers around 100–200 meV [25]. As for BH_4^- dynamics, the energy barrier is similar to what has been observed in the isostructural compounds $NaBH_4$ (≈ 120 meV) and KBH_4 (≈ 100 and 160 meV) [9,10]. In these alkali-metal borohydrides as well as in NH_4BH_4, the relatively large tetrahedral BH_4^- anion promotes the lowest-energy cubic crystallographic stacking,

leading to each cation in the structure being effectively nested within a pocket of six BH_4^- anions, with each BH_4^- anion straddling the smaller cation via two of its four hydrogen atoms [see Fig. 1(a)]. As such, one can expect each nested cation in the case of NH_4^+ to be able to reorient itself among a multitude of different positions without much steric interference by the straddling BH_4^- hydrogen atoms, leading to relatively low NH_4^+ reorientational barriers as observed. In contrast, the larger tetrahedral BH_4^- anions, which are surrounded by six nested NH_4^+ cations, will not be entirely free of steric interference from at least some of these cations upon reorientations between its two tetrahedral orientations in the structure, no matter how it performs the reorientation. Such steric interference is likely responsible, at least in part, for the observed higher BH_4^- energy barriers in these smaller-cation–larger-anion systems.

IV. CONCLUSION

In this QENS study we have investigated the nature of NH_4^+ and BH_4^- reorientational dynamics in ammonium borohydride, NH_4BH_4, both below and above the order-disorder polymorphic transition occurring between 45 and 50 K during heating. The results show that the transition to the disordered polymorph upon heating leads to dynamical changes corresponding to the onset of reorientational motions of the tetrahedral NH_4^+ cations, whereas at even higher temperatures (125 K), the tetrahedral BH_4^- anions also become dynamically active. The average relaxation time between successive molecular reorientations at 150 K is approximately 1 and 100 ps for the NH_4^+ cation and the BH_4^- anion, respectively. The ions also exhibit a large difference in their reorientational energy barriers, being approximately 10 meV for NH_4^+ and 100 meV for BH_4^-. The NH_4^+ dynamics at low temperatures (<125 K) can be adequately described as preferential tetrahedral tumbling, i.e., where each hydrogen atom can visit the four corners of the NH_4^+ tetrahedron, however, with reorientation around a specific axis more frequently occurring.

At temperatures higher than 125 K, the BH_4^- anion can be described as undergoing cubic tumbling, i.e., each hydrogen atom can visit the eight corners of a cube. In this higher-temperature regime, it is possible that the NH_4^+ dynamics evolves from tetrahedral tumbling motion, as observed at temperatures below 125 K, to either cubic tumbling or isotropic rotational diffusion motions. It is argued that the difference in relaxation mechanism for NH_4^+ and BH_4^- relates to the fact that NH_4^+ perceives the BH_4^- as static due to the large differences in relaxation time. Since each nearest-neighbor BH_4^- anion can assume two different orientations, this will give rise to different local noncubic energy landscapes for different NH_4^+ cations, leading to preferred NH_4^+ orientations. On the other hand, the BH_4^- anion will be subjected to an average cubic energy landscape and will thus adopt the observed disordered orientations imposed by the overall cubic symmetry of the lattice.

The increased understanding of how the reorientational dynamics of two or more active dynamical species affect one another is not only of fundamental interest, but also important for future development of hybrid solid-state superionic materials such as $Li_2(CB_9H_{10})(CB_{11}H_{12})$, and related compounds where it is known that the dynamical behavior of the substituent anions affects the long-range cation mobility [26].

The original data are accessible via the ISIS data cite [27].

[1] R. W. Parry, D. R. Schultz, and P. R. Girardot, J. Am. Chem. Soc. **80**, 1 (1958).

[2] P. Schouwink, M. B. Ley, A. Tissot, H. Hagemann, T. R. Jensen, L. Smrčok, and R. Černý, Nat. Commun. **5**, 5706 (2014).

[3] A. Karkamkar, S. M. Kathmann, G. K. Schenter, D. J. Heldebrant, N. Hess, M. Gutowski, and T. Autrey, Chem. Mater. **21**, 4356 (2009).

[4] T. K. Nielsen, A. Karkamkar, M. Bowden, F. Besenbacher, T. R. Jensen, and T. Autrey, Dalton Trans. **42**, 680 (2013).

[5] See Supplemental Material at http://link.aps.org/supplemental/10.1103/PhysRevMaterials.4.085002, which contains, crystal structure determined using PXRD, QENS spectra from 10 to 200 K, EISF model curves, as well as information of how the EISF for preferential tetrahedral tumbling was calculated.

[6] R. Flacau, C. I. Ratcliffe, S. Desgreniers, Y. Yao, D. D. Klug, P. Pallister, I. L. Moudrakovski, and J. A. Ripmeester, Chem. Commun. **46**, 9164 (2010).

[7] K. R. Ryan, A study of ammonia borane and its derivatives, Ph.D. thesis, University of Oxford, Oxford, UK, 2011.

[8] K. Hore, Ammonia borane and its derivatives: High weight percentage hydrogen storage materials, Ph.D. thesis, University of Oxford, Oxford, UK, 2013.

[9] N. Verdal, M. R. Hartman, T. Jenkins, D. J. DeVries, J. J. Rush, and T. J. Udovic, J. Phys. Chem. C **114**, 10027 (2010).

[10] A. Remhof, Z. Łodziana, P. Martelli, O. Friedrichs, A. Züttel, A. V. Skripov, J. P. Embs, and T. Strässle, Phys. Rev. B **81**, 214304 (2010).

[11] N. Verdal, T. J. Udovic, J. J. Rush, V. Stavila, H. Wu, W. Zhou, and T. Jenkins, J. Chem. Phys. **135**, 094501 (2011).

[12] M. Bée, *Quasielastic Neutron Scattering* (Adam Hilger, Bristol, 1988).

[13] B. Richter, J. B. Grinderslev, K. T. Møller, M. Paskevicius, and T. R. Jensen, Inorg. Chem. **57**, 10768 (2018).

[14] The identification of any commercial product or trade name does not imply endorsement or recommendation by the National Institute of Standards and Technology.

[15] P. Willmott, D. Meister, S. Leake, M. Lange, A. Bergamaschi, M. Böge, M. Calvi, C. Cancellieri, N. Casati, A. Cervellino *et al.*, J. Synchrotron Radiat. **20**, 667 (2013).

[16] S. Filippov, J. B. Grinderslev, M. S. Andersson, J. A. Armstrong, M. Karlsson, T. R. Jensen, S. I. Simak, and U. Häussermann, J. Phys. Chem. C **123**, 28631 (2019).

[17] K. Andersen, D. Martín y Marero, and M. Barlow, Appl. Phys. A: Mater. Sci. Process. **74**, s237 (2002).

[18] O. Arnold, J.-C. Bilheux, J. Borreguero, A. Buts, S. I. Campbell, L. Chapon, M. Doucet, N. Draper, R. F. Leal, M. Gigg *et al.*, Nucl. Instrum. Methods Phys. Res., Sect. A **764**, 156 (2014).

[19] R. T. Azuah, L. R. Kneller, Y. Qiu, P. L. Tregenna-Piggott, C. M. Brown, J. R. Copley, and R. M. Dimeo, J. Res. Natl. Inst. Stand. Technol. **114**, 341 (2009).

[20] T. J. Udovic, N. Verdal, J. J. Rush, D. J. De Vries, M. R. Hartman, J. J. Vajo, A. F. Gross, and A. V. Skripov, J. Alloys Compd. **580**, S47 (2013).

[21] T. Yildirim, P. M. Gehring, D. A. Neumann, P. E. Eaton, and T. Emrick, Phys. Rev. B **60**, 314 (1999).

[22] K. Sköld, J. Chem. Phys. **49**, 2443 (1968).

[23] J. J. Rush, L. A. de Graaf, and R. C. Livingston, J. Chem. Phys. **58**, 3439 (1973).

[24] B. Frick, J. Combet, and L. Van Eijck, Nucl. Instrum. Methods Phys. Res., Sect. A **669**, 7 (2012).

[25] H. Gutowsky, G. Pake, and R. Bersohn, J. Chem. Phys. **22**, 643 (1954).

[26] W. S. Tang, K. Yoshida, A. V. Soloninin, R. V. Skoryunov, O. A. Babanova, A. V. Skripov, M. Dimitrievska, V. Stavila, S. Orimo, and T. J. Udovic, ACS Energy Lett. **1**, 659 (2016).

[27] M. S. Andersson *et al.*, Dynamical properties of NH4BH4 studied using quasielastic neutron scattering, https://doi.org/10.5286/ISIS.E.RB1820371, STFC ISIS Neutron and Muon Source (2018).